WILEY | Hindawi

Research Article

An Improved Direct Torque Control with an Advanced Broken-Bar Fault Diagnosis for Induction Motor Drives

Oualid Aissa [ID],[1] **Abderrahim Reffas** [ID],[1] **Hicham Talhaoui** [ID],[1] **Djamel Ziane** [ID],[2] **and Abdelhakim Saim** [ID] [2]

[1]*LPMRN Laboratory, Faculty of Sciences and Technology, University Mohamed El Bachir El Ibrahimi of Bordj Bou Arreridj, El-Anasser, Algeria*
[2]*IREENA Laboratory, University of Nantes, Saint-Nazaire 44600, France*

Correspondence should be addressed to Djamel Ziane; djamel.ziane@univ-nantes.fr

This paper presents an advanced strategy combining fuzzy logic and artificial neural networks (ANNs) for direct torque control (DTC) and broken-bar fault diagnosis in induction motors. More specifically, a fuzzy-based controller is used to simultaneously minimize the stator flux and the electromagnetic torque ripples. A neural switching table is then proposed to achieve the interface inverter control. Besides, a closed-loop broken-bar fault detection strategy based on the Hilbert technique (HT) with the discrete wavelet transform (DWT) and ANNs is proposed. The fault detection is performed by analyzing the induction motor's stator current by using the combined techniques HT-DWT. The effect of a broken-bar fault on the machine varies according to the number and position of the broken bars. The neural detector was used in order to identify the number of broken bars through only one current measurement. The effectiveness of the developed control has been verified using MATLAB/Simulink and real-time simulation in OPAL-RT 4510. Obtained results show improved performances in terms of torque ripple minimization and stator current quality, evaluated, respectively, at 43.75% and 41.26% as well as a rigorous motor health monitoring.

1. Introduction

The induction machine is believed to be the electric machine most met these last years in the industrial sector due to its simplicity of design and maintenance, robustness of generation, reduced cost of manufacture, and reliability in operation [1]. Recently, the direct torque control (DTC) of the induction motor has become very useful in electric drives. Nevertheless, the induction motor is still affected by different types of faults. Monitoring the state of the induction motor driven in an open or closed loop is of imperious necessity, which prompted researchers to develop fault diagnosis techniques for this kind of motor [2, 3]. The objective of the diagnosis is to identify and locate the various problems of the motor to bring early solutions in order to increase its lifetime [4–6]. For the drives of the electrical machines, faults can be detected on the switches of the static converter connected to these machines. Electrical machines are subjected to various faults such as short circuits in the stator or breakage of one or more bars in the rotor [7, 8]. Similarly, the faults can also be encountered in measurement or detection elements [9].

The detection of anomalies and faults affecting the asynchronous machine was initially based on the analysis of noise, vibration, and temperature [10]. The high cost and noise sensitivity of the electromechanical installation have made these techniques impractical [11]. The second variety of technique recommended in the same order of idea is called the analysis of the signature of the motor current for which, each type of defect corresponds to it with a spectral signature [5, 6]. This method offers simplicity in the measurement of current and signal processing, which is fast Fourier transformation (FFT), characterized by its great ability in static mode to detect the anomaly of rotor bars breaking [11]. To overcome the problem of better frequency detection of the lateral bands due to proximity and overlap

with the fundamental frequency, the Hilbert transformation technique (HT) has been suggested [12]. On the other hand, the wavelet transform (WT) method is relevant to many areas of mathematics, including signal and image processing. It is considered as a suitable tool for the analysis of nonstationary signals [13].

The presence of variable speed drives controlling the induction machine makes it difficult to diagnose faults since the operation of the motor is always maintained in any desired requirements (speed references and load disturbances). The imposed regulation corrects and compensates the effect of the possible fault on the rotation speed of the asynchronous motor. For this reason, it is highly necessary to diagnose the defects of the closed-loop induction motor, which is widely used in the industrial sector, through the analysis of control variables other than those of the rotation speed [14, 15]. For the field-oriented control approach and the classical direct torque control strategy, the electrical quantities, which comprise the quadratic components of the current and the stator phase current as well as the mechanical quantity represented by the rotational speed (sensed or estimated), have been analyzed by the FFT, HT, or discrete wavelet transform (DWT) methods to extract the broken rotor bars fault of asynchronous motor. The authors in reference [4] have used the FFT technique and the DWT method for the identification of bar break defects applied to a reduced model of the asynchronous motor. In turn, the authors in reference [11] have used only the FFT method for the same type of fault affecting the same model of the asynchronous motor developed in reference [4]. By keeping the same control technique for the same model of the induction motor having the same defect studied in references [4, 11], the authors in reference [13] have applied the DWT method on the rotational speed, on the stator current, and on the signal coming from the speed regulator output to identify the possible anomalies. Another research work has been presented in reference [14] where the authors have proposed an indirect field-oriented control of the faulty induction motor. The HT and ANN methods have been employed for the fault diagnosis task. On one hand, the classical DTC strategy with an adaptive model of the asynchronous motor was investigated during the application of broken rotor bars faults. The FFT technique has treated the measured stator currents and voltages for the detection of the defect caused by the authors in reference [6]. On the other hand, the authors in reference [15] have conserved the use of the conventional DTC strategy of the induction motor with analysis of the stator current by FFT and DWT to diagnose the defect of broken bars. In recent years, the DTC control of healthy induction motors has seen the application of artificial intelligence and advanced control laws to improve its performance. Table 1 summarizes some of the techniques recently published in the literature.

Our research work proposes a new approach DTC of the induction motor, characterized by replacing the two hysteresis comparators of the flux and the torque and the switching table identified by three inputs and three outputs through a combined intelligent device. It is composed of a single fuzzy controller providing simultaneous flux and torque correction and a neural switching table where its first input represents the sector locating the position of the stator flux and its second is the output of the proposed fuzzy controller.

The same research work also proposes a diagnostic and fault detection study relating to a break of adjacent bars (1, 2, or 3) of the induction motor, characterized by its reduced model that can treat several types of defects, compared to other existing models. The information on the presence of defects is offered after analysis and examination of the stator current of the induction motor by the combined method between the Hilbert technique and the discrete wavelet transform (HT-DWT). In order to classify and detect the number of broken bars, artificial neural networks have been deployed in this work to perform this task. The necessary data for the intelligent neural detector are communicated by the HT-DWT transformation analyzing the stator current of the motor. The different results obtained with the consideration of the monitoring of possible faults for a closed-loop electric drive under different conditions confirm the ability of the induction motor to operate with better performance compared to the conventional DTC control.

This paper is organized into six sections. Section 2 is reserved for the presentation of the reduced mathematical model of the induction motor. The classical DTC strategy and the improved one based on artificial intelligence are discussed in detail in Section 3. Several simulation and experimental tests related to the improved DTC strategy of the healthy and faulty induction motor are exhibited and interpreted in Section 4. The applied techniques for the diagnosis, detection, and classification of the broken rotor bar fault affecting the induction motor are presented in Section 5. Finally, Section 6 concludes this paper.

2. Reduced Mathematical Model of Induction Motor

Each study of a physical mechanism obeys in most cases to a mathematical modeling. To know the behavior of the studied system under the action of different internal and external effects, a simulation is necessary to reveal the influence of existing or induced defects to better understand all the mechanisms governing the modeled system. The concretization of the reduced model intended to be applied for a closed-loop control with consideration of rotor and stator-related faults is extracted from the multiwinding model of the asynchronous motor as illustrated in Figure 1 [4, 11]. This model requires an extensive park transformation on the rotor system allowing having the system of (Nr) bars in reference (d, q). The developed model aims to study the behavior of the asynchronous motor in a healthy and defective state under different operating conditions [13].

The reduced system of the induction motor is modeled mathematically by the following equation:

$$[L_{\text{mot}}]\frac{d[I_{\text{mot}}]}{dt} = [U_{mot}] - [R_{\text{mot}}][I_{\text{mot}}]. \tag{1}$$

TABLE 1: Recent works on DTC control based on artificial intelligence and advanced strategies.

Recent works	Flux controller type	Torque controller type	Switching table type	Speed regulator type	Others
Reference [16]		Neural controller (3 inputs/3 outputs)			—
Reference [17]		—		Fuzzy controller	SVM strategy
Reference [18]	2 levels classical controller	3 levels classical controller	Classical table (3 inputs/ 3 outputs)	Optimized PID by the ACO algorithm	—
Reference [19]		—	—	Classical PI regulator	Optimized neural predictive control by PSO with the application of SVM strategy
Reference [20]		Fuzzy controller (3 inputs/3 outputs)		—	—
Reference [21]		—	—		Predictive control
Reference [22]	Fuzzy controller (2 inputs/1 output)		Modified table	Fuzzy controller	—
Reference [23]	Neural controller (2 inputs/1 output)	Neural controller (2 inputs/1 output)	Classical table (3 inputs/3 outputs)	Classical PI regulator	—

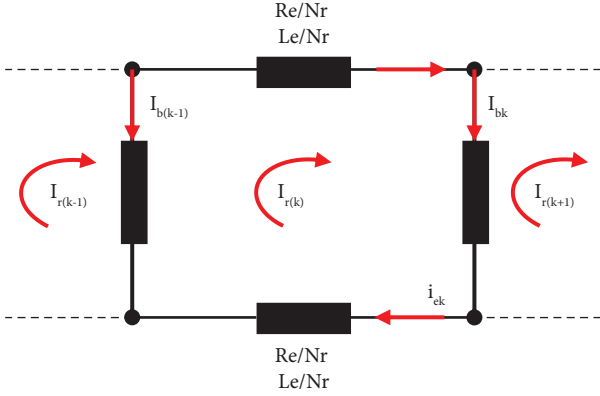SVM, space vector modulation; ACO, ant colony optimization; PSO, particle swarm optimization.

FIGURE 1: Equivalent circuit relating to the rotor of the induction motor.

The matrices of the voltages (U_{mot}), currents (I_{mot}), inductances (L_{mot}), and resistors (R_{mot}) of the motor are, respectively, defined as follows:

$$[U_{\mathrm{mot}}] = [U_{ds}\, U_{qs}]^T,$$

$$[I_{\mathrm{mot}}] = [I_{ds}\, I_{qs}\, I_{dr}\, I_{dr}\, I_e]^T,$$

$$[L_{\mathrm{mot}}] = \begin{bmatrix} L_{sc} & 0 & -\dfrac{N_r}{2}M_{sr} & 0 & 0 \\[2mm] 0 & L_{sc} & 0 & -\dfrac{N_r}{2}M_{sr} & 0 \\[2mm] -\dfrac{3}{2}M_{sr} & 0 & L_{rc} & 0 & 0 \\[2mm] 0 & -\dfrac{3}{2}M_{sr} & 0 & L_{rc} & 0 \\[2mm] 0 & 0 & 0 & 0 & L_e \end{bmatrix},$$

$$[R_{\mathrm{mot}}] = \begin{bmatrix} R_s & -\omega L_{sc} & 0 & \dfrac{N_r}{2}\omega M_{sr} & 0 \\[2mm] \omega L_{sc} & R_s & -\dfrac{N_r}{2}\omega M_{sr} & 0 & 0 \\[2mm] 0 & 0 & [R_{\mathrm{rdd}} & R_{\mathrm{rdq}}] & 0 \\[2mm] 0 & 0 & [R_{\mathrm{rqd}} & R_{\mathrm{rqq}}] & 0 \\[2mm] 0 & 0 & 0 & 0 & R_e \end{bmatrix},$$

where (L_{sc}) represents the total cyclic inductance of the stator phase, composed of the magnetization inductance

(L_{sp}) and the leakage inductance (L_{sf}), which is represented as follows:

$$L_{sc} = L_{sp} + L_{sf}. \tag{3}$$

Now, the magnetization inductance (L_{sp}) is calculated as follows:

$$L_{sp} = 4\mu_0 \cdot \left(\frac{N_s^2 \cdot R \cdot l}{e \cdot p^2 \cdot \pi} \right). \tag{4}$$

The mutual inductance (M_{sr}) relative to the two stator and rotor parts is expressed by using the following equation:

$$M_{sr} = \left(\frac{4}{\pi} \right) \cdot \left(\frac{\mu_0}{e.p^2} \right) \cdot N_s \cdot R \cdot l \sin \left(\frac{\alpha}{2} \right). \tag{5}$$

The electrical angle (α) of two adjacent meshes of the rotor is calculated by using the following relation:

$$\alpha = p \cdot \left(\frac{2\pi}{N_r} \right). \tag{6}$$

The cyclic inductance of the rotor phase (L_{rc}) is represented by the following equation:

$$L_{rc} = L_{rp} - M_{rr} + 2 \cdot \left(\frac{L_e}{N_r} \right) + 2 \cdot L_e \cdot (1 - \cos \alpha). \tag{7}$$

The identification of the cyclic inductance of the rotor phase (L_{rc}) is subordinated to the knowledge of the inductance of the rotor mesh (L_{rp}) and the mutual inductance of nonadjacent rotor meshes (M_{rr}). These two inductances are, respectively, defined as follows:

$$L_{rp} = \left(\frac{N_r - 1}{N_r^2} \right) \cdot \left(\frac{\mu_0}{e} \right) \cdot 2\pi \cdot R \cdot l,$$

$$M_{rr} = -\left(\frac{1}{N_r^2} \right) \cdot \left(\frac{\mu_0}{e} \right) \cdot 2\pi \cdot R \cdot l. \tag{8}$$

The electromagnetic torque generated by the reduced model of the induction motor, expressed as a function of the stator and rotor currents, is formulated by the following equation:

$$T_{em} = \frac{3}{2} \cdot P \cdot N_r.M_{sr} \cdot \left(I_{ds}.I_{qr} - I_{qs}.I_{dr} \right). \tag{9}$$

The rotor speed (ω_r) of the induction motor depending on the electromagnetic torque is identified as follows:

$$\frac{d\omega_r}{dt} = \frac{1}{J} \left(T_{em} - T_r - f\omega_r \right), \tag{10}$$

where J, T_r, and f are, respectively, the inertia moment, torque resistance, and friction coefficient.

The expressions that take into account the problem of breakage of the rotor bars of the induction motor are given by the following relationships:

$$\begin{cases} R_{\text{rdd,rqq}} = R_r + \dfrac{2}{N_r}\,(1 - \cos\alpha)\sum_k R_{bfk}\cdot(1 \pm \cos\,(2k-1)\cdot\alpha), \\[4mm] R_{\text{rdq,rqd}} = -\dfrac{2}{N_r}\,(1 - \cos\alpha)\sum_k R_{bfk}\cdot\sin\,(2k-1)\cdot\alpha. \end{cases} \tag{11}$$

Through the aforementioned system of equations, the algebraic sum concerns all the bars with defects. The term (R_{bfk}) denotes the initial value before the defect of the index bar (k). When using the induction motor with a reduced model exposed to defects, controlled by intelligent DTC strategy, it is necessary to transfer useful quantities positioned in the reference (d, q) to the fixed reference (α, β) characterizing the DTC approach.

3. Proposed DTC Strategy

The classical DTC control is a technique that essentially deals with the direct regulation of the electromagnetic torque once the stator currents and voltages of the asynchronous motor are measured. Two conventional hysteresis controllers with two and three levels are used, respectively, to ensure proper control of the stator flux and electromagnetic torque after estimating and comparing these two quantities with their corresponding references. The electromagnetic torque reference is generated at the output of the standard proportional-integral (PI) controller. The same controller also provides effective speed control of the induction motor. On the other hand, as presented in Table 2, this control approach has a standard commutation table with three inputs (stator flux position, torque, and flux correction actions) and three outputs (S_a, S_b, and S_c), acting as the switching control of the inverter feeding the induction motor. The following equations are required for this control law [22, 24]:

$$\begin{cases} \overset{\wedge}{\phi}_{s\alpha} = \displaystyle\int_0^t \left(V_{s\alpha} - R_s\cdot I_{s\alpha}\right)\mathrm{d}t, \\[4mm] \overset{\wedge}{\phi}_{s\beta} = \displaystyle\int_0^t \left(V_{s\beta} - R_s\cdot I_{s\beta}\right)\mathrm{d}t. \end{cases} \tag{12}$$

The module and the position of the stator flux are, respectively, calculated as follows:

$$\begin{aligned} \overset{\wedge}{\phi}_s &= \sqrt{\overset{\wedge}{\phi}_{s\alpha}{}^2 + \overset{\wedge}{\phi}_{s\beta}{}^2}, \\[3mm] \overset{\wedge}{\theta}_s &= \tan^{-1}\left(\frac{\overset{\wedge}{\phi}_{s\beta}}{\overset{\wedge}{\phi}_{s\alpha}}\right). \end{aligned} \tag{13}$$

Only after determining the two quantities of flux and stator current, as given in the following relationship, can the electromagnetic torque be calculated:

$$\hat{T}_{em} = P\cdot\left(\overset{\wedge}{\phi}_{s\alpha}\cdot I_{s\beta} - \overset{\wedge}{\phi}_{s\beta}\cdot I_{s\alpha}\right), \tag{14}$$

where P denotes the asynchronous motor's number of pole pairs.

3.1. Design of Fuzzy Torque and Flux Controllers. The researcher Zadeh invented the principle of fuzzy sets in 1965 [25]. Thereafter, the principles of this invention were applied by the researcher Mamdani in 1974 in order to design the first controller based on the fuzzy logic theory [26]. Its simplicity of structure and its robustness have given it a great reputation to be used in several fields of research; among them, we will mention the field of electrical engineering. To properly operate this kind of controller, three essential steps must be followed, namely, fuzzification, fuzzy inference process, and defuzzification [22, 26]. The enhanced DTC is characterized by a flux and torque control that operates simultaneously by using a fuzzy controller called fuzzy torque and flux controller (FTFC) that will replace the two standard two-level and three-level flux and torque controllers, respectively. The main function of the FTFC is to minimize the ripples of the stator flux and electromagnetic torque, thus inducing to obtain better performance of the DTC control.

The developed FTFC is of the Mamdani type. It is characterized by two inputs which are the difference recorded between the reference electromagnetic torque (recovered at the output of the conventional PI-type speed controller) and the estimated electromagnetic torque as well as the difference resulting from the difference between the reference stator flux and the estimated flux. These two inputs are fuzzified, respectively, by five and three triangular-type membership functions for the torque error and the flux error. The output of the fuzzy controller, which represents the flux and torque correction actions at the same time, is in turn fuzzified by five very narrow triangular-type membership functions. Based on Table 3, the fuzzy rules characterizing our FTFC controller are formulated by a set of if-then expressions, as follows:

$$\begin{cases} \text{Fuzzy rule (1): If Torque Error is NB and Flux Error is N Then: FTFC is RedT RedF,} \\[2mm] \text{Fuzzy rule (2): If Torque Error is NB and Flux Error is Z Then: FTFC is RedT IncF,} \\[2mm] \quad\vdots \\[2mm] \text{Fuzzy rule (15): If Torque Error is PB and Flux Error is P Then: FTFC is IncT IncF.} \end{cases} \tag{15}$$

TABLE 2: Standard switching table.

			Sector					
			1	2	3	4	5	6
	1		V_2	V_3	V_4	V_5	V_6	V_1
	0	1	V_7	V_0	V_7	V_0	V_7	V_0
Torque	−1	Flux	V_6	V_1	V_2	V_3	V_4	V_5
correction	1	correction	V_3	V_4	V_5	V_6	V_1	V_2
	0	0	V_0	V_7	V_0	V_7	V_0	V_7
	−1		V_5	V_6	V_1	V_2	V_3	V_4

V_0 (000); V_1 (100); V_2 (110); V_3 (010); V_4 (011); V_5 (001); V_6 (101); V_7 (111).

TABLE 3: FTFC controller rules.

Torque error		NB	NS	Z	PS	PB
	N	RedT RedF	RedT RedF	KC	IncT RedF	IncT RedF
Flux error	Z	RedT IncF	RedT RedF	KC	IncT RedF	IncT RedF
	P	RedT IncF	RedT IncF	KC	IncT IncF	IncT IncF

N, negative; Z, zero; P, positive; B, big; S, small; Inc, increase; Red, reduce; KC, keep constant; T, torque; F, flux.

These rules constitute a database connecting the two inputs with the output for selecting a good decision-making after execution of the defuzzification phase by the center of gravity method, as illustrated in Figure 2.

3.2. Design of Neural Decision Table for the Smart DTC Strategy.

Inspired typically by the highly evolved functionality of the human brain, ANNs have invaded the field of advanced electrical drives considerably [23]. With the capacity to learn from already existing systems, this intelligent technique is able to regenerate new generalized models that can adapt to situations that have not been considered during the learning phase [27]. The neuron endowed with activation and summation function represents the essential part of the ANN. The mathematical model of the neuron is given by the following relationship [16]:

$$Y = \xi \left(\sum_{i=1}^{m} W_i \cdot X_i \lambda \right), \tag{16}$$

where the neuron's input and output signals are identified by $X_1, X_2, \ldots, X_m$ and Y, respectively, the weights associated with the neuron's inputs are represented by $W_1, W_2, \ldots, W_m$, and λ denotes the neuron's bias while ξ is the tangent sigmoid function.

The supervised learning algorithm is very important when creating the ANN. In fact, the backpropagation method alternating between forward and backward motion is the most commonly used. The calculation of the mean square error (E_r) for this technique is given by the following equation:

$$E_r(l) = \frac{1}{m} \sum_{i=1}^{m} \left(S_i(l) - Y_i(l) \right)^2, \tag{17}$$

where l determines the number of iterations, m represents the input-output training data, S_i is the desired response, and Y_i is the output provided by the neural network in response to the input X_i.
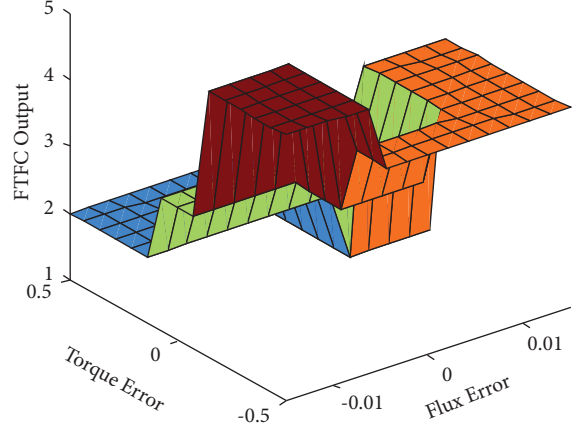

FIGURE 2: FTFC controller map.

The update of the weights of the neural network output layer is expressed by the following equation:

$$W_{ji}(l+1) = W_{ji}(l) - \mu \frac{\partial E_r(l)}{\partial W_{ji}(l)}, \tag{18}$$

where μ designates the learning rate and W_{ji} represents the weight linking the jth neuron of the output layer to the ith neuron of the previous layer.

The high values of μ accelerate the learning phase of the ANN and lead to a rapid convergence. To do this, a positive constant η known as the moment constant must be added to equation (18) to get the following equation:

$$W_{ji}(l+1) = W_{ji}(l) - \mu \frac{\partial E_r(l)}{\partial W_{ji}(l)} + \eta \Delta W_{ji}(l). \tag{19}$$

The neural switching table has been developed based on the standard switching table of the DTC strategy. The proposed fuzzy corrector of torque and flux has been designed to operate with a specific switching table of two inputs as depicted in Table 4.

The neural decision table proposed in this paper has been integrated into the improved DTC strategy to be able to work properly with the fuzzy controller (FTFC), leading to the development of a combined fuzzy neural DTC (FNDTC) strategy, ensuring effective control of the induction motor.

As shown in Figure 3, the constructed neural decision table has a basic architecture (3-16-3), ensuring the best learning and testing performance. It is composed of an input layer of 03 neurons representing sector, torque, and flux correction actions; a hidden layer of 16 neurons with Tansig activating functions; and an output layer of 03 neurons representing the three decision actions (S_a, S_b, and S_c) with purelin activating functions. The supervised learning method applied is that of Levenberg–Marquardt while the method of calculating the error is that of the least squares with a number of iterations of 1000 and an acceptable tolerance of the error fixed to 10^{-4}.

The advanced FNDTC strategy of the induction motor, characterized by the combination of two intelligent controllers of the fuzzy and neural type, which is intended to

TABLE 4: Fuzzy switching table.

Torque and flux correction	Sector					
	1	2	3	4	5	6
IncT IncF	V_2	V_3	V_4	V_5	V_6	V_1
IncT RedF	V_3	V_4	V_5	V_6	V_1	V_2
KC	V_0	V_7	V_0	V_7	V_0	V_7
RedT RedF	V_5	V_6	V_1	V_2	V_3	V_4
RedT IncF	V_1	V_2	V_3	V_4	V_5	V_6

Inc, increase; Red, reduce; KC, keep constant; T, torque; F, flux.
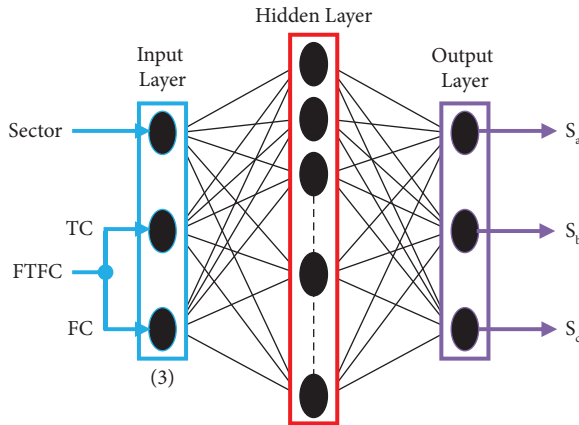
FIGURE 3: Neural architecture of the proposed decision table.

improve the performance of the standard DTC, is illustrated in Figure 4.

4. Real-Time Simulation and Discussions

The effectiveness of the proposed control strategy has been tested using real-time simulations in OPAL-RT 4510. The entire control strategy and system have been implemented in the MATLAB/Simulink environment and built-in OPAL-RT 4510 using RT-LAB. Indeed, after obtaining the simulation results in MATLAB/Simulink software, a real-time validation is carried out using an OPAL-RT. An OPAL-RT-4510 rapid control prototyping system is used for real-time simulation. This setup comprises of the target computing nodes, an oscilloscope, a host PC, an Ethernet communication link, and input and output boards. The setup is a part of the smart power platform of the IRENA laboratory. Figure 5 depicts the laboratory setup used for testing. The necessary parameters used for these tests are presented in Table 5.

The induction motor in healthy and faulty states is driven under load at high and low speeds of 200 rad/s and 30 rad/s for the two directions of rotation as shown in Figure 6. The motor in this case has a defect of two adjacent broken bars at the instant $t = 1.5$ s. It is clearly visible that the induction motor was able to reject the disturbance of the load caused at time $t = 1$ s on the one hand and suitably follow the references of the imposed rotation speeds in this robustness test at times $t = 2, 4,$ and 6 s on the other hand.

Through Figure 7, it can be seen that the electromagnetic torque and the stator current (I_{sa}) react positively to the realized robustness tests. Furthermore, the spectral analysis carried out on the stator current (I_{sa}) for the different imposed rotation speeds of 200 rad/s, −200 rad/s, 30 rad/s, and −30 rad/s gave us, respectively, the improved THD rates of 8.75%, 7.66%, 11.66%, and 12.28% compared to those of the classical DTC which had the values of 22.95%, 22.91%, 25.88%, and 26.08%. These values represent an average improvement rate of 41.26% for the stator's current quality. For the stator flux, it is always kept constant at its reference value of 1 Wb.

The classical DTC and suggested FNDTC techniques have been validated and compared in real-time using the hardware in the loop test method based on both dSPACE 1103 and OPAL-RT 4510 devices. As presented in Figure 8, the response of the induction motor rotational speed under load presents better speed dynamics with a minimal overshoot and a static error of very low value with perfect tracking of its reference value of 200 rad/s.

The disturbance caused was quickly rejected thanks to the intervention of the speed regulator employed in this command. From the same figure, it is obvious that at startup, the electromagnetic torque reaches its maximum value limited to 7 N·m and then stabilizes at a value practically zero in a steady state (without load). After the motor is loaded with a resistive torque of 3.5 N·m, for which the electromagnetic torque reacts suitably to this provoked action, the torque ripples recorded when applying the FNDTC strategy are reduced in a very significant way compared to those given by the classical DTC (reduced from ±1.6 N·m to ±0.7 N·m giving an improvement rate of 43.75%). With regard to the stator current of phase (a) shown in Figure 8, a good sinusoidal shape was obtained when using the intelligent DTC, with an experimental THD value of 8.99% as recorded in Figure 9. In addition, for both control strategies, the stator current of phase (a) reacts correctly after loading the induction motor by a resistive torque of 3.5 N·m, as indicated in Figure 8.

To prove the effectiveness of the FNDTC strategy, the loaded healthy and faulty asynchronous motor has been driven under a variety of desired speeds. As shown in Figure 10, the rotation speed was able to follow the different imposed references with success due to the applied control law.

The obtained experimental results show that the proposed DTC approach, applied to the healthy and faulty induction motor, is able to minimize the ripples of the electromagnetic torque in a very effective manner, thus ensuring a better quality of the stator currents compared to the classical DTC strategy. Nevertheless, the knowledge of the existence of the fault that affected the asynchronous motor through these results is not apparent.

5. Methodology of Rotor Fault Diagnosis

5.1. Theoretical Study. In this paper, the diagnostic approach for identifying rotor faults (broken rotor bars) in an induction machine is performed through the combined
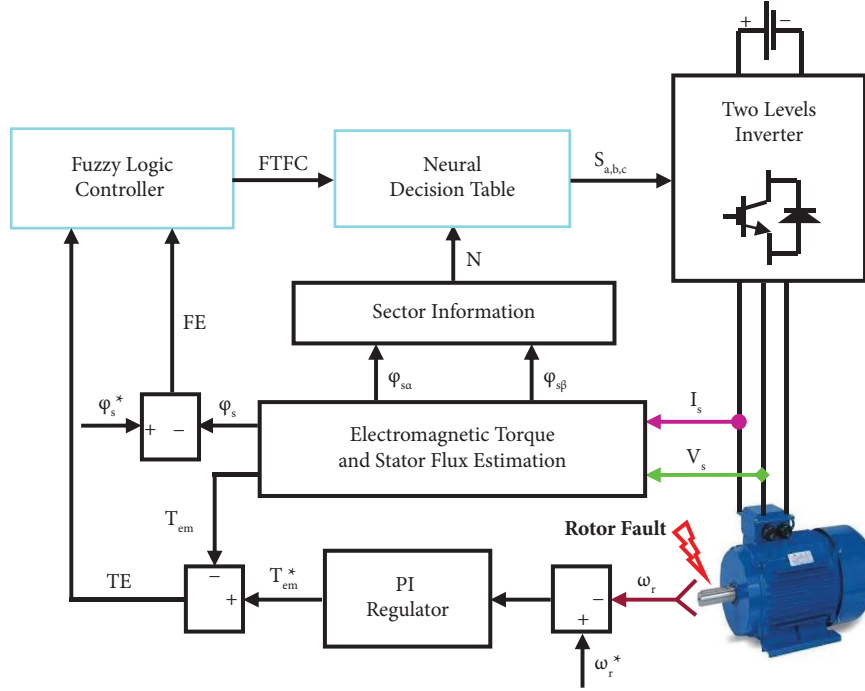
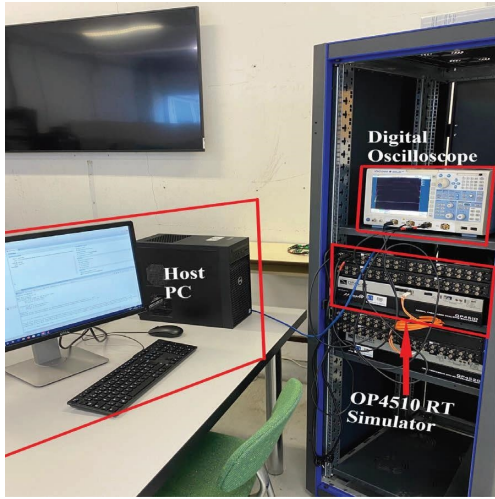Figure 4: Block diagram of the FNDTC strategy.

Figure 5: Real-time simulation test bench.

Table 5: Specifications of simulation and experimental parameters.

P_n: nominal power	1.1 kW
V: nominal line voltage	220 V
I: nominal current	4.6 A
f_s: power source frequency	50 Hz
P: number of pole pairs	1
R: average radius of the air-gap	35.76 mm
l: rotor length	65 mm
e: mean diameter of air-gap	0.2 mm
μ_0: magnetic permeability of the air	$4\pi * 10^{-7}$ H/m
N_r: number of bars	16
N_s: number of turns per phase	160
R_s: stator phase resistance	$7.58\,\Omega$
R_r: rotor bar resistance	$150\,\mu\Omega$
R_e: ring portion resistance	$150\,\mu\Omega$
L_e: short-circuit ring leakage inductance	$0.1\,\mu$H
L_b: leakage inductance of a rotor bar	$0.1\,\mu$H
L_{fs}: stator leakage inductance	26.5 mH
J: inertia moment	$5.4 * 10^{-3}$ kg·m^2
T_s: sampling time	0.0001 s
Simulation software	MATLAB/ Simulink
Practical implementation system (HIL tests)	OPAL-RT 4510

HT-DWT method as shown in Figure 11. By using this methodology, faults can be diagnosed automatically. It depends on the use and analysis of the stator current, which is used as input to the developed neural network detector as indicated in Figure 11.

The Hilbert transform is a convolution dependent on the time factor of the signal $F(t)$ with the function $(1/t)$ and highlights the specific characteristics of the signal $F(t)$ in the following manner [14]:

$$HT[F(t)] = \frac{1}{\pi} \int_{-\infty}^{+\infty} \frac{F(\tau)}{t - \tau} d\tau = F(t) * \frac{1}{\pi t}, \qquad (20)$$

where the time, the time domain signal, the convolution, and the transformation of $F(t)$ by Hilbert are, respectively, represented by t, $F(t)$, $*$, and HT $[F(t)]$.

For the DWT analysis method, it is based on the conversion of signals in the time/frequency domain. This method depends on the use of filters with different frequencies where they divide the analysis signal into two others: the first is called the approximation signal, which is
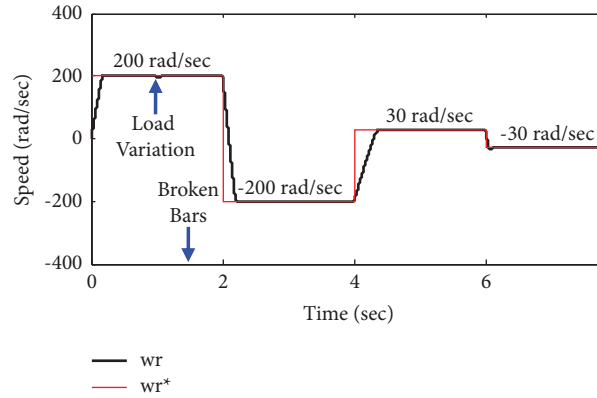
FIGURE 6: Simulation results of the induction motor rotation speed based on the FNDTC strategy.
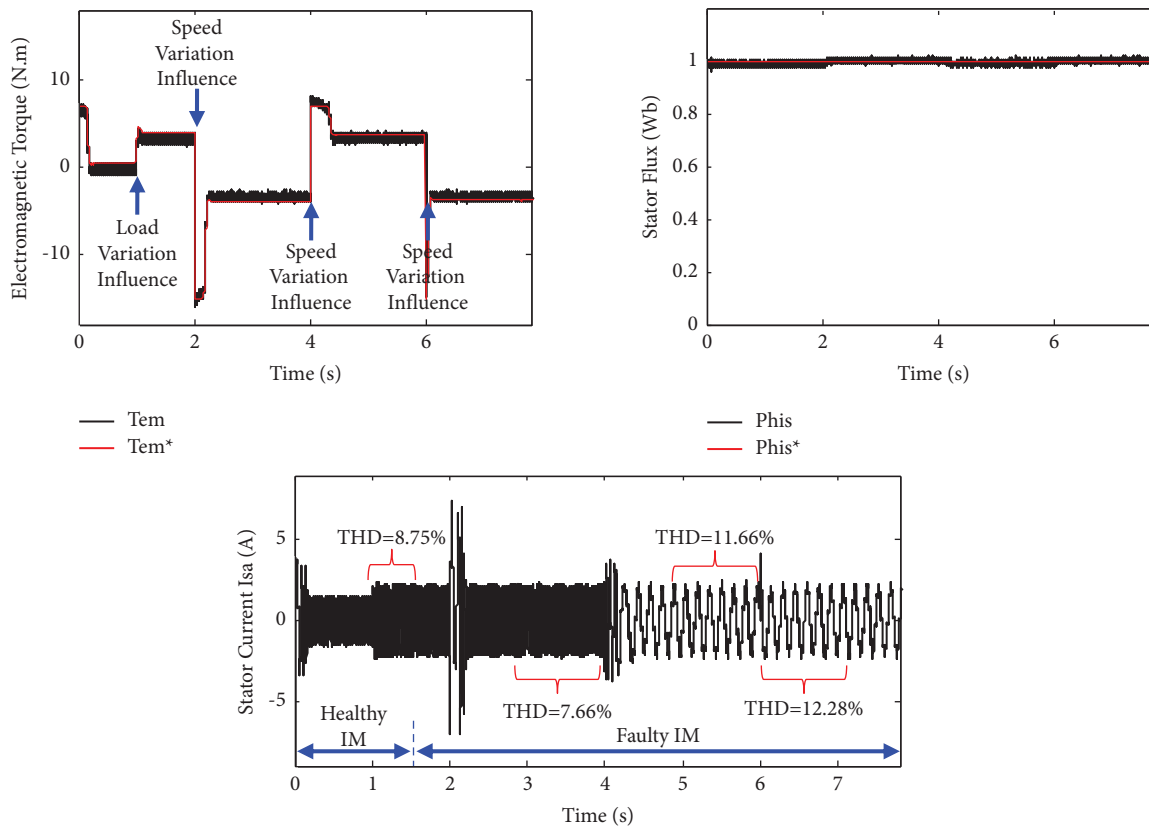

FIGURE 7: Simulation results: electromagnetic torque, stator flux, and stator current (I_{sa}) of the FNDTC strategy.

produced by the low-pass filter and the second is called the detail signal, which in turn is produced by the high-pass filter [4, 28].

5.2. Verification of Applied Techniques. Using simulation and experiment data, the stator current and its formulated envelope via Hilbert's analysis for a motor loaded by a nominal load in the healthy state and broken-bars (b.b) faulted state are shown in Figures 12(a) and 12(b).

One of the most important advantages of Hilbert analysis (envelope) is the suppression of the fundamental frequency (f_i). It is considered a problem when diagnosing

broken rotor bar faults, especially when the load or speed is low. In this situation, the fundamental frequency and the frequency of the fault are near each other, which makes it difficult to identify faults [29].

From Figures 12(a) and 12(b), we can see that it is very difficult to detect the fault by observing only the performance of the machine in the time domain. Signal analysis by FFT is one of the most important solutions to facilitate fault diagnosis, since it converts the time domain into the frequency domain. The benefit of this procedure is that each defect has its unique frequency. Therefore, the extracted frequencies can diagnose the fault that manifests in the machine as shown in
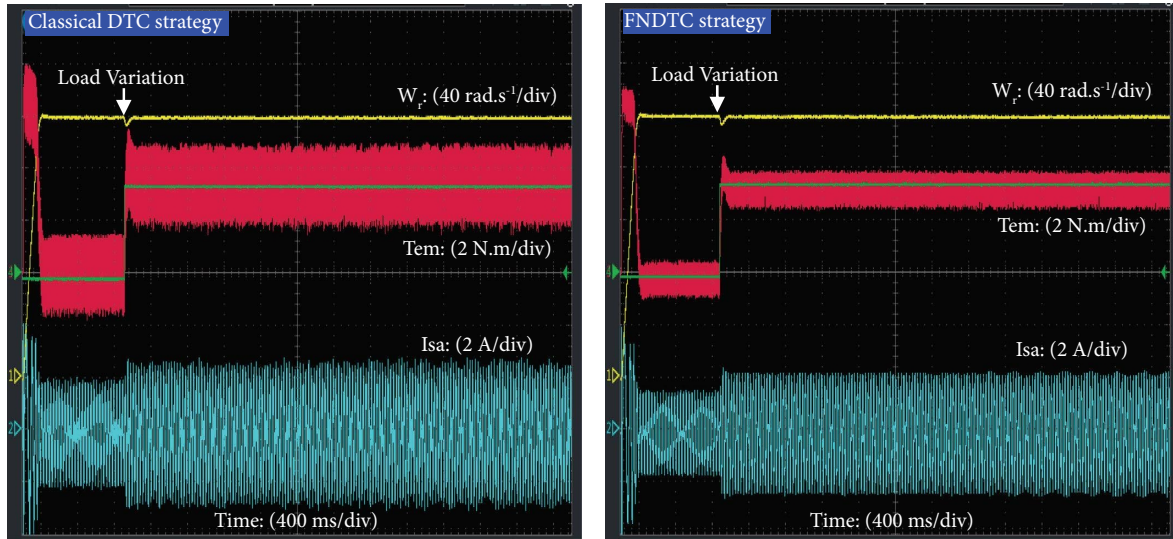
FIGURE 8: Experimental results: rotation speed, electromagnetic torque, and stator current (I_{sa}) of the classical and FNDTC strategies.
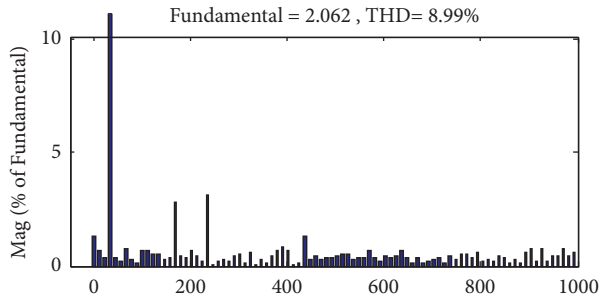

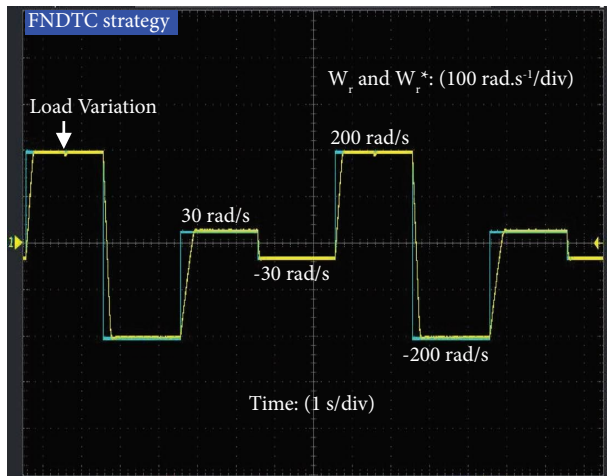FIGURE 9: Spectral analysis of the FNDTC strategy stator current.

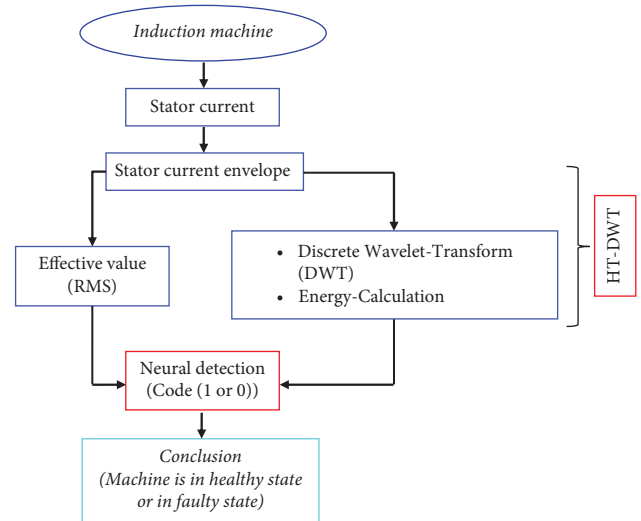FIGURE 10: Experimental result of the induction motor rotation speed based on the FNDTC strategy.

FIGURE 11: Diagnostic methodology based on HT-DWT.

a broken rotor bar fault in the induction machine. The following equation expresses these additional harmonics or frequencies [29]:

$$f_{H.fault} = 2\,K\,S_i\,f_i, \tag{21}$$

where $K = 1, 2, 3, \ldots, f_i$ is the machine's frequency and S_i is the motor's slip.

The frequency values found from Figures 13(a) and 13(b) and calculated using equation (21) are close to each other, as seen in Table 6.

Through the previously mentioned advantageous aspects, Hilbert's analysis is very useful for diagnosing defects. The fundamental drawback of this approach is that it does not operate well on unstable signals (nonstationary), for example, when the machine is operating at different loads, variable speeds, or faults during startup. In fact, when the signal is not constant, it creates several other frequencies,

Figures 13(a) and 13(b). From the same figures, we analyzed the stator current of the induction motor in the healthy and faulty state using the HT-FFT method.

Through the comparison between the two Figures 13(a) and 13(b), we notice that there are additional frequencies when the machine is faulty, which indicates the existence of
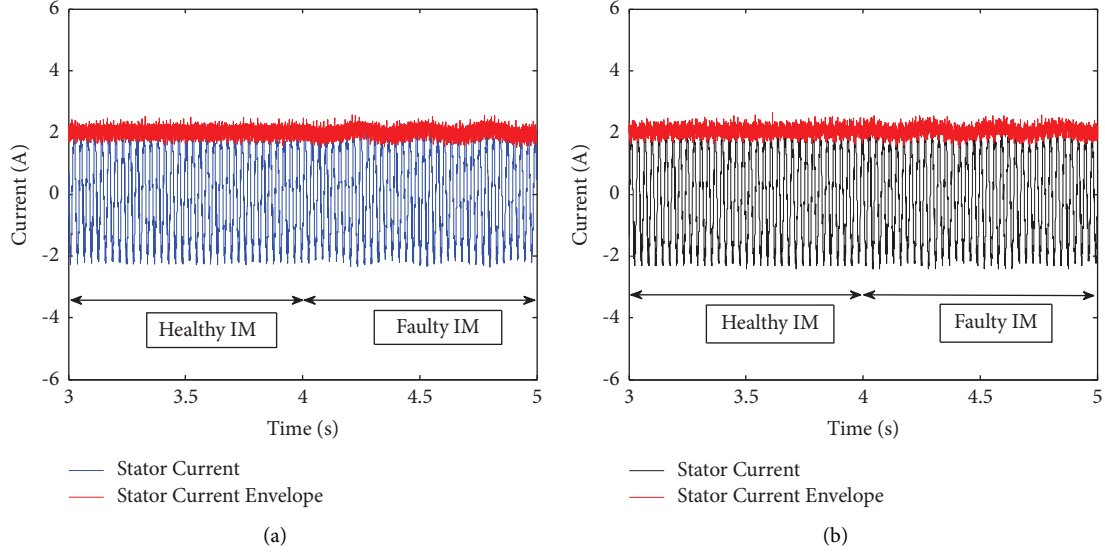
FIGURE 12: Stator current and its envelope in the healthy state and in fault of 2.b.b: (a) simulation results and (b) experimental data.
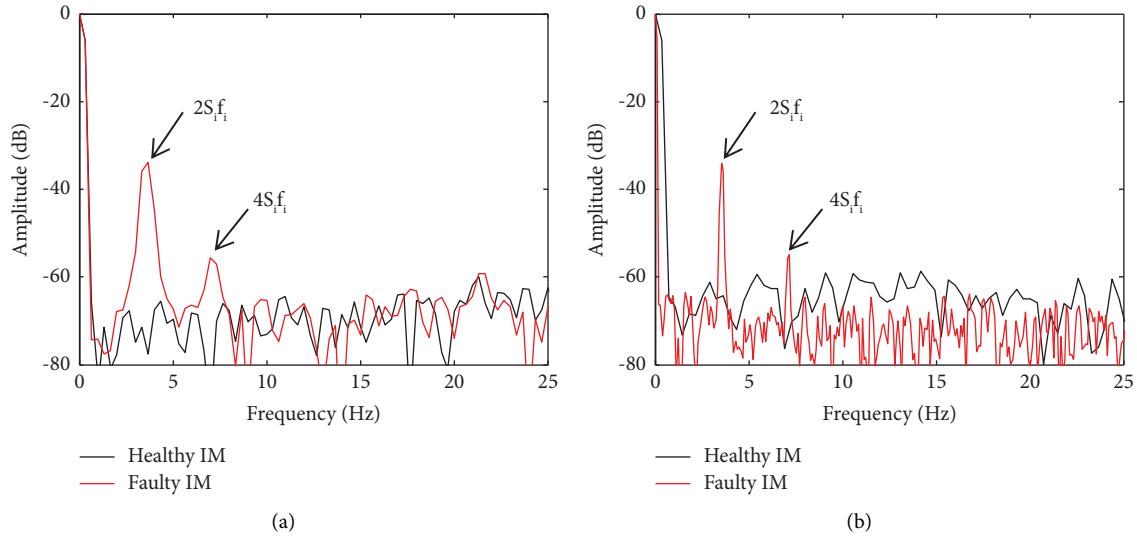

FIGURE 13: HT-FFT of stator current in the healthy state and in fault of 2.b.b: (a) simulation results and (b) experimental data.

TABLE 6: Frequencies of the results obtained from the simulation and experimental spectrum of the machine with a fault of 2.b.b.

	Simulation tests		Experimental tests	
	$2S_i f_i$	$4S_i f_i$	$2S_i f_i$	$4S_i f_i$
$f_{H.\text{fault}}$ (Hz): deduced	3.667	7	3.531	7.156
$f_{H.\text{fault}}$ (Hz): calculated	3.643	7.286	3.538	7.077
Magnitude (dB)	−33.86	−55.62	−33.99	−54.88

which causes difficulties in determining the fault frequencies. The HT-DWT approach has been recommended to solve this main problem.

In order to calculate the level (N_{Li}) of decomposition of the DWT method, the sampling frequency (f_{sa}) and the network frequency (f_{ne}) affect this level. It can be determined by using the following equation [4, 28]:

$$N_{Li} > \frac{\log(f_{sa}/f_{ne})}{\log(2)} + 1. \tag{22}$$

In this study, the decomposition level is set at 9, as shown in Table 7.

The current signal (Sig) analyses by the HT-DWT method in the healthy and defective states are compared in Figure 14(a) (simulation results) and Figure 14(b) (experimental data). It can be seen that when a fault occurs, the

$N_{Li} = 9$	Frequency (Hz)
a9	0 to 9.7656
d9	9.7656 to 19.53125
d8	19.53125 to 39.0625
d7	39.0625 to 78.125
d6	78.125 to 156.25
d5	156.25 to 312.5
d4	312.5 to 625
d3	625 to 1250
d2	1250 to 2500
d1	2500 to 5000

amplitude of the a9 coefficients increases, as shown by the comparison of the details and signals of the approximation in the following two cases: healthy and faulty. The a9 coefficient can be used as an indicator to diagnose this fault.

5.3. Intelligent Fault Detector.

Automatic diagnosis is one of the most important applications that have attracted the interest of researchers for several considerations, including facilitating the process of fault identification and diagnosis in the induction motor based on artificial intelligence. The neural network is one of the most important methods of artificial intelligence. To discover and get the best performance from the neural network structure, we perform a number of tests [29].

The neural network employed in this section is made up of three layers: an input layer, a layer for decision-making as an output, and a hidden layer made up of five neurons. The RMS values of the current envelope $Ia_{(E.RMS)}$ and energy (E_{a9}) are considered as inputs to this network. For the output, we use two pairs of numbers that contain a number of zero (0) or one (1), where each number represents the probability that the machine is in a healthy state or in a faulty state (healthy (0.b.b), one broken rotor bar (1.b.b), two broken rotor bars (2.b.b), and three broken bars (3.b.b or >2.b.b)), as shown in Figure 15.

The two entries, Energy (E_{a9}) and $Ia_{(E.RMS)}$, were chosen for several considerations, including the following:

(i) They are affected by the change of state of the machine, from a healthy machine to a faulty one, and even when the fault changes, i.e., when the number of broken rotor bars increases (Figure 16)

(ii) In addition, one of the most important reasons to choose them is that despite the change in the load of the machine, the fault can be detected, which means that the load does not affect the fault detection (Figure 16)

In order to model an intelligent approach to diagnosing the fault, a diverse database must be created that allows us to detect the fault accurately and easily, as shown in Figure 17. Several samples were taken from the machine in several cases (healthy, 1.b.b, 2.b.b, and 3.b.b or >2.b.b) and different loads (10%, 20%, 40%, 60%, 80%, and 100% of rated load), as shown in Figure 17.

As presented in Figure 18, a root-mean-square error (RMSE) of $1.5567e^{-11}$ and 65 iterations are required to finish the learning phase. The recorded RMSE value is very close to zero. We can therefore consider that the learning stage of the intelligent fault detector is effective.

The targets, response of the intelligent fault detector, and output errors are shown in Figure 19. It can be seen that the network response follows the targets with the same path and the same code. As indicated in Figure 19, the learning error value which is about 10^{-5} reflects the good learning quality of the designed neural detector model.

Different values not found in the previous database (learning and training phase) are taken in order to test the behavior of the suggested and developed neural fault detector. The test is performed as follows:

(i) From $t = 0$ s to $t = 1$ s, there is no fault in the motor and the load value is equal to 30% of the rated load value

(ii) From $t = 1$ s to $t = 2$ s, there is no fault in the motor and the load value is equal to 90% of the rated load value

(iii) From $t = 2$ s to $t = 3$ s, there is a fault in the motor (1.b.b) and the load value is equal to 30% of the rated load value

(iv) From $t = 3$ s to $t = 4$ s, there is a fault in the motor (1.b.b) and the load value is equal to 50% of the rated load value

(v) From $t = 4$ s to $t = 5$ s, there is a fault in the motor (2.b.b) and the load value is equal to 50% of the rated load value

(vi) From $t = 5$ s to $t = 6$ s, there is a fault in the motor (2.b.b) and the load value is equal to 70% of the rated load value

(vii) From $t = 6$ s to $t = 7$ s, there is a fault in the motor (>2.b.b) and the load value is equal to 30% of the rated load value

(viii) From $t = 7$ s to $t = 8$ s, there is a fault in the motor (>2.b.b) and the load value is equal to 70% of the rated load value.

Figure 20 shows the outputs and the errors of these outputs when testing the neural fault detector under the previously mentioned values. Through the performed tests and obtained results, we can remark that the suggested neural detector is able to automatically detect faults, especially when loading the machine under different loads.

Finally, a synthesis including a comparative study between the proposed fault diagnosis strategy and existing methods in the literature is shown in Table 8. From Table 8, it can be seen that the closed-loop fault diagnosis strategy proposed in this paper is better than the diagnosis methods
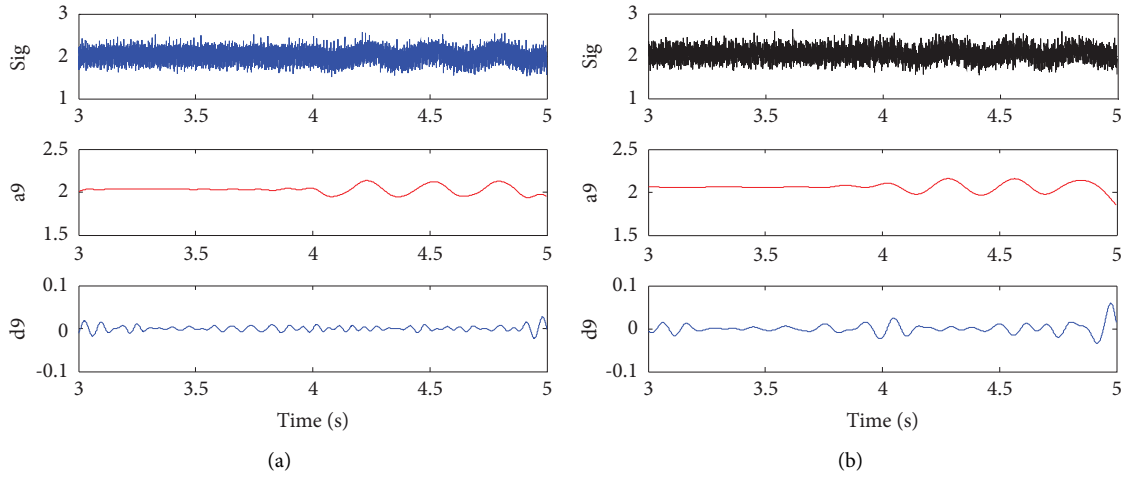
FIGURE 14: HT-DWT method of stator current in the healthy state and in fault of 2.b.b: (a) simulation results and (b) experimental data.
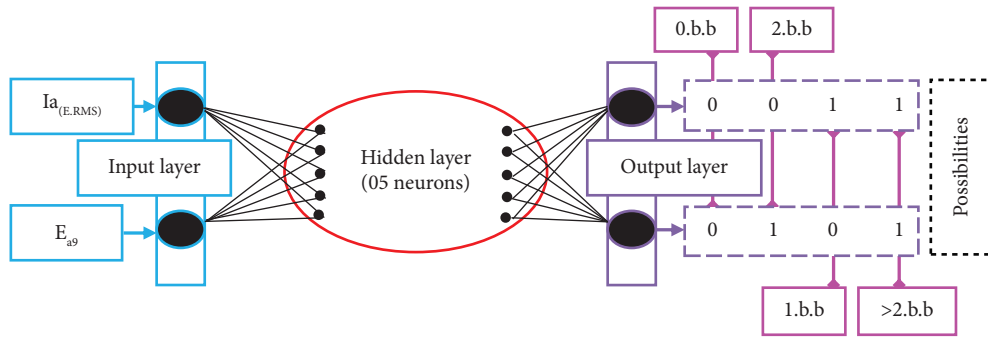

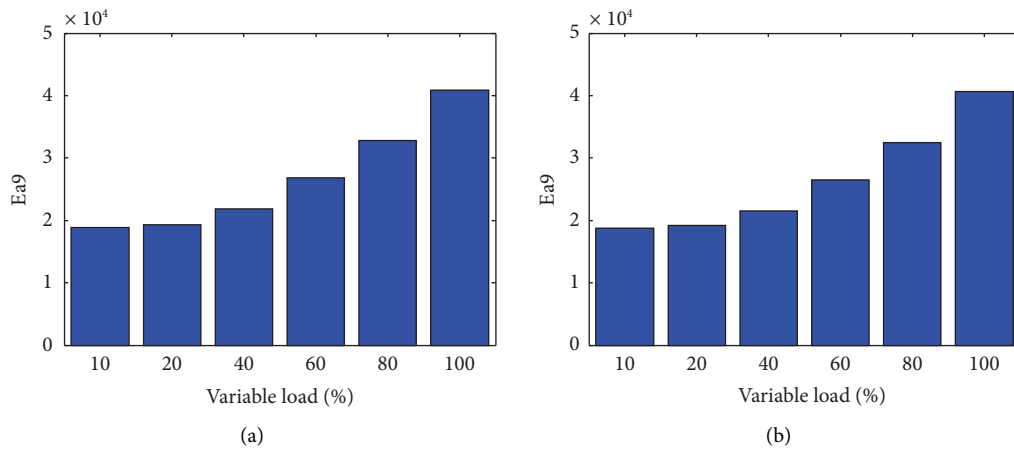FIGURE 15: Neural network methodology applied for fault diagnosis.
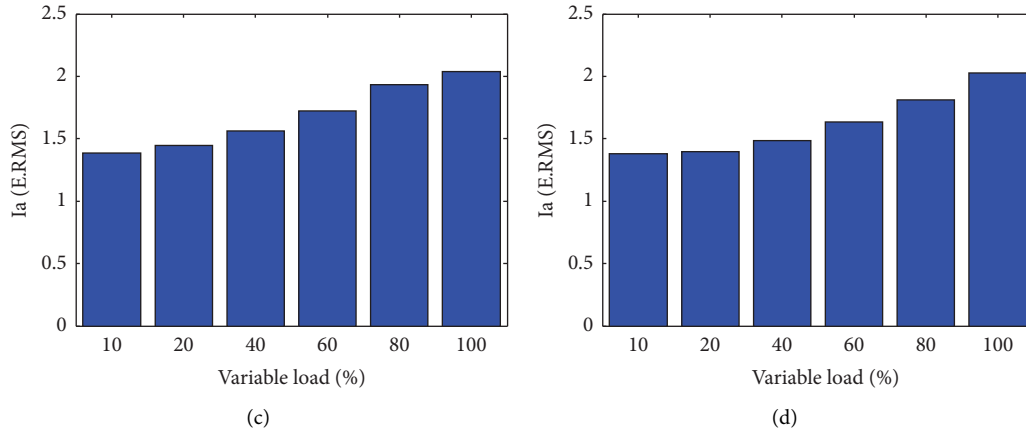

(a)

(b)

FIGURE 16: Continued.

(c)

(d)

FIGURE 16: E_{a9} and Ia$_{(E.RMS)}$ at different torque values: (a, c) healthy IM and (b, d) faulty IM (2.b.b).
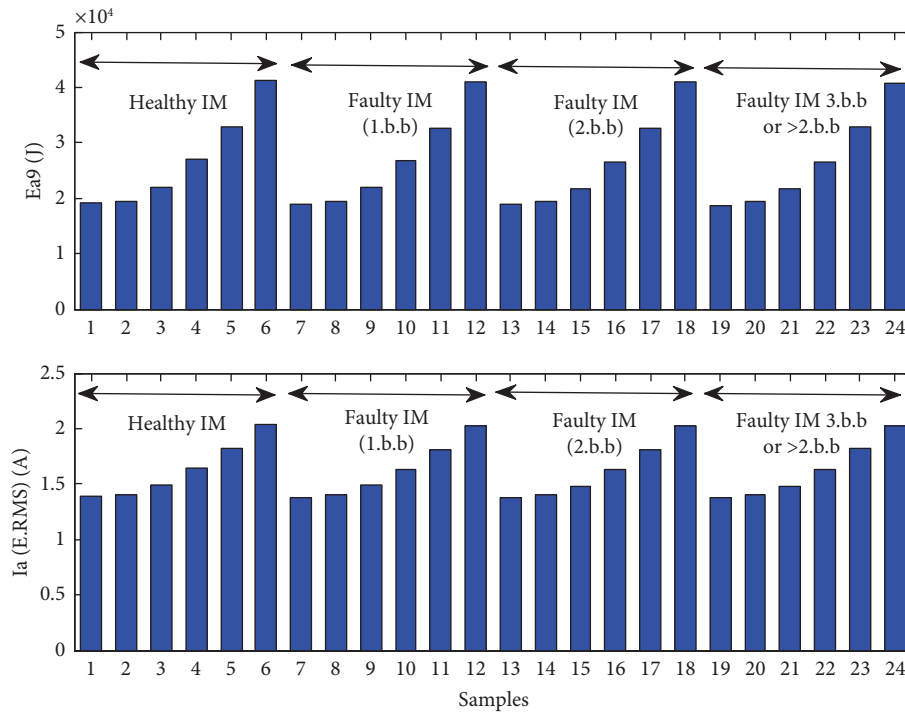

FIGURE 17: Neural network's training set's input data.

recently published in the literature. The combined HT-DWT diagnostic method that we have applied to the induction motor is functional for stationary, nonstationary, full-load, and low-load conditions. In addition, the defect affecting the induction motor is automatically detected by a neural detector. By referring to the recently published research works

of Table 8, it is clear that these works do not provide a diagnosis in all conditions compared to our proposed diagnosis and detection methods. On the other hand, the FNDTC control applied to both the healthy and the faulty induction motor is the most suitable to ensure an effective speed regulation.

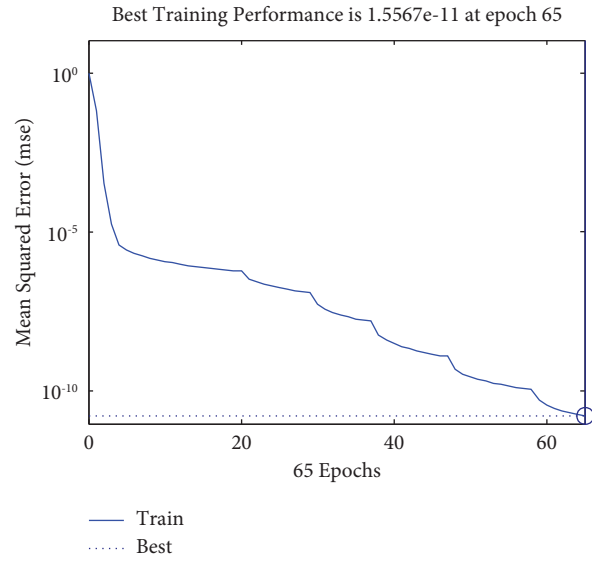Best Training Performance is 1.5567e-11 at epoch 65
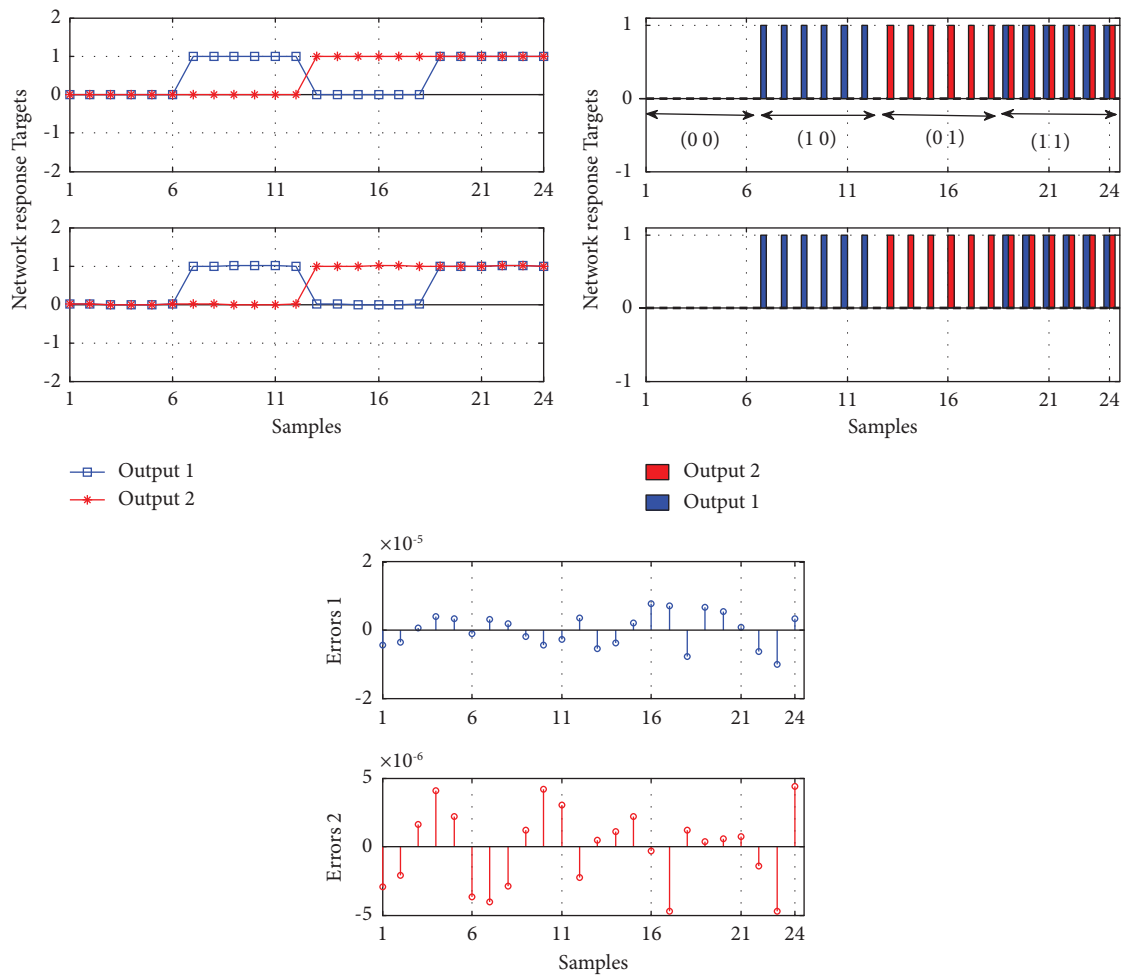
Figure 18: Recorded RMSE value.

Figure 19: Targets, network response, and output errors of the suggested neural detector.
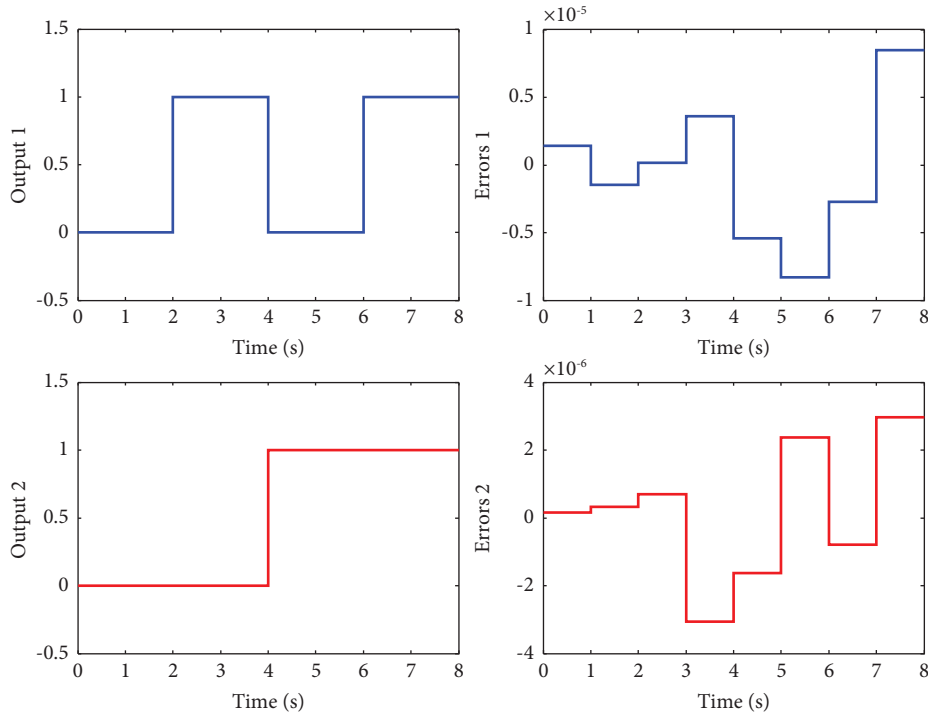
FIGURE 20: Outputs and errors of these outputs when testing the suggested neural detector.

TABLE 8: Comparative study between the proposed fault diagnosis strategy and existing methods in the literature.

Recent works	IM control strategies	Applied diagnostic methods	Operation modes		Load type		Automatic fault detection
			Stationary	Nonstationary	Full	Low	
Proposed work	Closed-loop drive fuzzy neural DTC	Combined HT-DWT	Yes	Yes	Yes	Yes	ANN detector
Reference [2]	Open-loop drive	DWT and HT	Yes	Yes	Yes	—	No
Reference [6]	Closed-loop drive classical DTC	FFT	Yes	No	Yes	Yes	No
Reference [10]	Open-loop drive	DWT	Yes	Yes	Yes	—	ANN detector
Reference [11]	Closed-loop drive FOC	FFT	Yes	No	Yes	—	No
Reference [14]	Closed-loop drive IFOC	HT	Yes	No	Yes	Yes	ANN detector
Reference [15]	Closed-loop drive classical DTC	FFT and DWT	Yes	Yes	Yes	—	No
Reference [30]	Open-loop drive	Wavelet packet	Yes	Yes	Yes	Yes	Fuzzy logic detector

6. Conclusion

The monitoring of the state of health for the induction motor driven in a closed loop by an improved DTC strategy with consideration of the load variation was discussed in this paper. Furthermore, an intelligent broken bars number detector based on artificial neural networks has been proposed. Simulation and real-time testing in OPAL-RT have been carried out in order to highlight the effectiveness of the proposed strategy under different operating conditions of the asynchronous motor. The new configuration of the DTC strategy based on the fuzzy logic and artificial neural network controllers has improved the quality of the stator currents while minimizing the undulations of the electromagnetic torque. An average improved rate of 41.26% has been recorded for the stator current, while the electromagnetic torque undulations have achieved a rate of 43.75%.

Concerning the induction motor health, the stator current analysis via the combined method between the Hilbert technique and the discrete wavelet transform has been realized for the purpose of detecting any broken bar defects in the rotor of the driven motor. The real-time tests have confirmed the effectiveness of the suggested method in the field of fault diagnosis of the induction motor controlled by the enhanced DTC strategy.

Finally, as a continuation of this research work, it is envisaged to apply an advanced control law in order to operate

the induction motor controlled by the DTC at a fixed switching frequency and to study other types of faults such as eccentricity and stator winding short-circuit, affecting the induction motor.

Acronyms

IM:	Induction motor
DTC:	Direct torque control
FOC:	Field-oriented control
IFOC:	Indirect field-oriented control
SVM:	Space vector modulation
ANN:	Artificial neural network
ACO:	Ant colony optimization
PSO:	Particle swarm optimization
HT:	Hilbert transform
DWT:	Discrete wavelet transform
FFT:	Fast Fourier transformation
FTFC:	Fuzzy torque and flux controller
FNDTC:	Fuzzy neural direct torque control
Mot:	motor
s, r:	Stator and rotor index
d, q:	Direct and quadratic components
U_{ds}, U_{qs}:	Stator voltages in (d, q) axis
I_{ds}, I_{qs}:	Stator currents in (d, q) axis
I_e:	Short-circuit ring current
N_r:	Number of rotor bars
L_e:	Short-circuit ring leakage inductance
μ_0:	Magnetic permeability of the air
N_s:	Number of turns per phase
R:	Average radius of the air-gap
l:	Rotor length
e:	Mean diameter of the air-gap
α:	Angle between two broken rotor bars
R_s:	Stator resistance
R_r:	Rotor resistance
L:	Inductance
M:	Mutual inductance
P:	Number of pole pairs
Tem:	Electromagnetic torque
ωr:	Rotor speed
PI:	Proportional integrator
α, β:	Fixed reference frame axes
Isα, Isβ:	Stator currents in the fixed reference frame (α, β)
Vsα, Vsβ:	Stator voltages in the fixed reference frame (α, β)
$\varphi s\alpha$, $\varphi s\beta$:	Stator flux in the fixed reference frame (α, β)
θ_s:	Stator flux angle
S_a, S_b, S_C:	Inverter control actions
b.b:	Broken bars
THD:	Total harmonic distortion
Sig:	Signal
E:	Energy.

Data Availability

The necessary data are included in the paper.

Conflicts of Interest

The authors declare that they have no conflicts of interest regarding the publication of this article.

Acknowledgments

References

[1] L. Schreier, J. Bendl, and M. Chomat, "Analysis of stator and rotor currents and torque of induction machine with rotor-bar faults," *Electrical Engineering*, vol. 103, no. 1, pp. 519–528, 2021.

[2] H. Zhu, Z. Jia, X. Song, and W. Sun, "An approach to detect broken rotor bars based on instantaneous frequency of the fault characteristic harmonic during the start-up transient," *The International Journal of Advanced Manufacturing Technology*, vol. 124, no. 11-12, pp. 4107–4119, 2023.

[3] C. Chakraborty and V. Verma, "Speed and current sensor fault detection and isolation technique for induction motor drive using axes transformation," *IEEE Transactions on Industrial Electronics*, vol. 62, no. 3, pp. 1943–1954, 2015.

[4] H. Talhaoui, A. Menacer, A. Kessal, and R. Kechida, "Fast Fourier and discrete wavelet transforms applied to sensorless vector control induction motor for rotor bar faults diagnosis," *ISA Transactions*, vol. 53, no. 5, pp. 1639–1649, 2014.

[5] M. A. Moussa, M. Boucherma, and A. Khezzar, "A detection method for induction motor bar fault using sidelobes leakage phenomenon of the sliding discrete Fourier transform," *IEEE Transactions on Power Electronics*, vol. 32, no. 7, pp. 5560–5572, 2017.

[6] T. Goktas and M. Arkan, "Discerning broken rotor bar failure from low frequency load torque oscillation in DTC induction motor drives," *Transactions of the Institute of Measurement and Control*, vol. 40, no. 1, pp. 279–286, 2018.

[7] J. Zhang, S. Li, and Z. Xiang, "Adaptive fuzzy finite-time fault-tolerant control for switched nonlinear large-scale systems with actuator and sensor faults," *Journal of the Franklin Institute*, vol. 357, no. 16, pp. 11629–11644, 2020.

[8] M. O. Mustafa, D. Varagnolo, G. Nikolakopoulos, and T. Gustafsson, "Detecting broken rotor bars in induction motors with model-based support vector classifiers," *Control Engineering Practice*, vol. 52, pp. 15–23, 2016.

[9] Y. Yu, Y. Zhao, B. Wang, X. Huang, and D. Xu, "Current sensor fault diagnosis and tolerant control for VSI-based induction motor drives," *IEEE Transactions on Power Electronics*, vol. 33, no. 5, pp. 4238–4248, 2018.

[10] M. Defdaf, F. Berrabah, A. Chebabhi, and B. D. E. Cherif, "A new transform discrete wavelet technique based on artificial neural network for induction motor broken rotor bar faults diagnosis," *International Transactions on Electrical Energy Systems*, vol. 31, no. 4, Article ID e12807, 2021.

[11] T. Ameid, A. Menacer, H. Talhaoui, and I. Harzelli, "Broken rotor bar fault diagnosis using fast Fourier transform applied to field-oriented control induction machine: simulation and

experimental study," *The International Journal of Advanced Manufacturing Technology*, vol. 92, no. 1-4, pp. 917–928, 2017.

[12] P. Gangsar and R. Tiwari, "A support vector machine based fault diagnostics of induction motors for practical situation of multi-sensor limited data case," *Measurement*, vol. 135, pp. 694–711, 2019.

[13] T. Ameid, A. Menacer, H. Talhaoui, and Y. Azzoug, "Discrete wavelet transform and energy eigen value for rotor bars fault detection in variable speed field-oriented control of induction motor drive," *ISA Transactions*, vol. 79, pp. 217–231, 2018.

[14] R. Senthil Kumar, I. Gerald Christopher Raj, I. Alhamrouni et al., "A combined HT and ANN based early broken bar fault diagnosis approach for IFOC fed induction motor drive," *Alexandria Engineering Journal*, vol. 66, pp. 15–30, 2023.

[15] R. Senthil Kumar and I. Gerald Christopher Raj, "Broken rotor bar fault detection using DWT and energy eigenvalue for DTC fed induction motor drive," *International Journal of Electronics*, vol. 108, no. 8, pp. 1401–1425, 2021.

[16] S. Gdaim, A. Mtibaa, and M. F. Mimouni, "Artificial neural network-based DTC of an induction machine with experimental implementation on FPGA," *Engineering Applications of Artificial Intelligence*, vol. 121, Article ID 105972, 2023.

[17] A. Aoufi, A. Bourek, and I. Ghadbane, "Real time implementation of fuzzy logic based direct torque control of three phase induction motor," *Przeglad Elektrotechniczny*, vol. 2, pp. 100–103, 2023.

[18] S. Mahfoud, A. Derouich, A. Iqbal, and N. El Ouanjli, "ANT-colony optimization-direct torque control for a doubly fed induction motor: an experimental validation," *Energy Reports*, vol. 8, pp. 81–98, 2022.

[19] A. Sahu, K. B. Mohanty, and R. N. Mishra, "Development and experimental realization of an adaptive neural-based discrete model predictive direct torque and flux controller for induction motor drive," *Applied Soft Computing*, vol. 108, Article ID 107418, 2021.

[20] M. Errouha, A. Derouich, S. Motahhir, O. Zamzoum, N. El Ouanjli, and A. El Ghzizal, "Optimization and control of water pumping PV systems using fuzzy logic controller," *Energy Reports*, vol. 5, pp. 853–865, 2019.

[21] A. Ammar, B. Talbi, T. Ameid, Y. Azzoug, and A. Kerrache, "Predictive direct torque control with reduced ripples for induction motor drive based on T-S fuzzy speed controller," *Asian Journal of Control*, vol. 21, no. 4, pp. 2155–2166, 2019.

[22] O. Aissa, S. Moulahoum, I. Colak, N. Kabache, and B. Babes, "Improved performance and power quality of direct torque control of asynchronous motor by using intelligent controllers," *Electric Power Components and Systems*, vol. 44, no. 4, pp. 343–358, 2016.

[23] K. Bouhoune, K. Yazid, M. S. Boucherit, and B. N. Mobarakeh, "Simple and efficient direct torque control of induction motor based on artificial neural networks," in *Proceedings of the IEEE International Conference on Electrical Systems for Aircraft, Railway, Ship Propulsion and Road Vehicles & International Transportation Electrification Conference*, Nottingham, UK, November 2018.

[24] I. M. Alsofyani, N. R. N. Idris, and K. B. Lee, "Dynamic hysteresis torque band for improving the performance of lookup-table-based DTC of induction machines," *IEEE Transactions on Power Electronics*, vol. 33, no. 9, pp. 7959–7970, 2018.

[25] L. A. Zadeh, "Fuzzy sets," *Information and Control*, vol. 8, no. 3, pp. 338–353, 1965.

[26] O. Aissa, S. Moulahoum, I. Colak, B. Babes, and N. Kabache, "Design and real time implementation of three-phase three switches three levels Vienna rectifier based on intelligent controllers," *Applied Soft Computing*, vol. 56, pp. 158–172, 2017.

[27] T. S. Murthy and T. V. Kiran, "Comparative analysis of fuzzy DTC and ANN DTC for induction motor," *International Journal of Emerging Trends in Engineering and Development*, vol. 2, pp. 483–493, 2013.

[28] A. Bouzida, O. Touhami, R. Ibtiouen, A. Belouchrani, M. Fadel, and A. Rezzoug, "Fault diagnosis in industrial induction machines through discrete wavelet transform," *IEEE Transactions on Industrial Electronics*, vol. 58, no. 9, pp. 4385–4395, 2011.

[29] B. Bessam, A. Menacer, M. Boumehraz, and H. Cherif, "Detection of broken rotor bar faults in induction motor at low load using neural network," *ISA Transactions*, vol. 64, pp. 241–246, 2016.

[30] H. Talhaoui, T. Ameid, O. Aissa, and A. Kessal, "Wavelet packet and fuzzy logic theory for automatic fault detection in induction motor," *Soft Computing*, vol. 26, no. 21, pp. 11935–11949, 2022.